Suppression of Quenching in Plasmon-Enhanced Luminescence *via* Rapid Intraparticle Energy Transfer in Doped Quantum Dots

Yerok Park,[†] Arika Pravitasari,[†] Jeffery E. Raymond,[‡] James D. Batteas,[†,*] and Dong Hee Son[†,*]

[†]Department of Chemistry, Texas A&M University, College Station, Texas 77842, United States and [‡]Laboratory for Synthetic-Biologic Interactions, Department of Chemistry, Texas A&M University, College Station, Texas 77842, United States

ABSTRACT We show the suppression of luminescence quenching by metal nanoparticles (MNPs) in the plasmon enhancement of luminescence *via* fast sensitized energy transfer in Mn-doped quantum dots (QDs). The rapid intraparticle energy transfer between exciton and Mn, occurring on a few picoseconds time scale, separates the absorber (exciton) from the emitter (Mn), whose emission is detuned far from the plasmon of the MNP. The rapid temporal separation of the absorber and emitter combined with the reduced spectral overlap between Mn and plasmonic MNP suppresses the quenching of the luminescence while taking advantage of the plasmon-enhanced excitation. We compared the plasmon enhancement of exciton and Mn luminescence intensities in undoped and doped QDs simultaneously as a function of the distance between MNP and QD layers in a multilayer structure to examine the expected advantage of the reduced quenching in the sensitized luminescence. At the optimum MNP–QD layer distance, Mn luminescence exhibits stronger net enhancement than that of the exciton, which can be explained with a model incorporating fast sensitization along with reduced emitter–MNP spectral overlap. This study demonstrates that materials exhibiting fast sensitized luminescence that is sufficiently red-shifted from that of the sensitizer can be superior to usual luminophores in harvesting plasmon enhancement of luminescence by suppressing quenching.

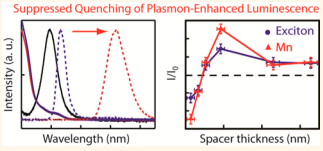

KEYWORDS: doped semiconducting nanocrystals · plasmonics

Enhancement of excitation or emission rates by noble metal nanostructures adjacent to a luminophore has been widely utilized as a way to increase the intensity of photoluminescence (PL) or electroluminescence.[1−9] The enhancement of absorption or emission rate resulting in a stronger luminescence arises from the enhanced local electric field by the localized surface plasmon or the modification of the photonic mode and local dielectric environment in the vicinity of the metal nanostructures.[5,10,11] Enhancement of excitation has been extensively studied particularly with colloidal metal nanoparticles (MNPs) that exhibit strong plasmon resonance, due to the relatively easy synthesis of MNPs with widely tunable resonances in the visible and near IR spectral region.[12−14] While such MNPs can enhance the excitation of luminophores *via* enhanced local electric fields, at close distances they can also quench the luminescence through energy transfer from the excited luminophore to the MNPs.[15−18] Because of the relatively broad plasmon spectrum of MNPs compared to the Stokes-shifted luminescence of typical luminophores, simultaneous enhancement of the two opposing processes, *i.e.*, excitation and quenching of emission, is unavoidable in most cases. For this reason, the difference in the MNP–luminophore distance dependence of the excitation enhancement and luminescence quenching has been exploited to optimize the net plasmonic enhancement of the luminescence.[1,18,19]

Here, we show that the MNP-induced quenching of the luminescence from semiconductor quantum dots (QDs) can be partially suppressed *via* fast intraparticle exciton–dopant energy transfer in doped QDs, resulting in a stronger net plasmon enhancement of the luminescence. This is shown in Mn-doped CdS/ZnS QDs that exhibit sensitized Mn luminescence *via* fast exciton–Mn energy transfer occurring on a few picoseconds time scale.[20,21] The sensitized Mn luminescence is significantly more red-shifted

* Address correspondence to dhson@chem.tamu.edu; batteas@chem.tamu.edu.

Received for review May 21, 2013 and accepted November 4, 2013.

Published online November 04, 2013
10.1021/nn405101h

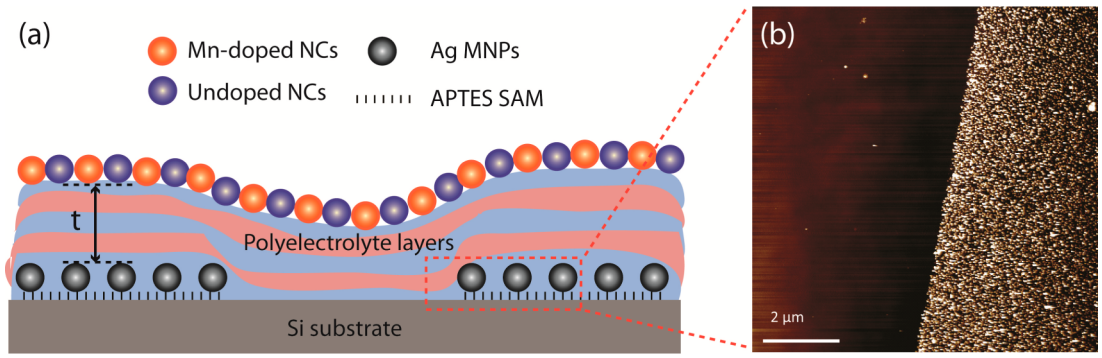

Figure 1. (a) Multilayer structure fabricated on Si substrate used for the comparison of plasmon enhancement of exciton and Mn luminescence. (b) AFM image of the patterned Ag MNP layer on Si substrate before adding spacer and QD layer.

from both the exciton absorption and plasmon resonance of the MNP than exciton luminescence. Therefore, the fast exciton–Mn energy transfer process that rapidly separates the absorber (exciton) and emitter (Mn) can reduce the spectral overlap between the emitter and plasmon resonance of MNPs.[22] One might anticipate that such reduction in emitter–MNP spectral overlap will suppress MNP-induced quenching of the luminescence, leading to a stronger net plasmon enhancement of the luminescence in doped QDs compared to undoped QDs. In order to verify the expected advantage from sensitized luminescence, here we made a systematic comparison of luminescence enhancement by Ag-MNPs for both Mn-doped and undoped CdS/ZnS QDs. To examine this, the net plasmon-enhanced luminescence of doped and undoped QDs were measured simultaneously as a function of the average distance between a mixed layer of the two types of QDs and Ag MNP layer formed on a Si substrate using a patterned array of the Ag MNPs we have described in previous studies of plasmon-enhanced luminescence of QDs (Figure 1).[23] In this comparison, Mn luminescence in doped QDs exhibited a stronger net enhancement than exciton luminescence in undoped QDs at an optimum QD–MNP distance of *ca.* 10 nm. At very short QD–MNP distances (*ca.* 2 nm) however, Mn luminescence exhibited a stronger net quenching than exciton luminescence. These observations can be described qualitatively using a kinetic model, accounting for all of the competing processes including exciton–Mn energy transfer and MNP-induced quenching of both exciton and Mn luminescence. The present study suggests that the sensitized luminescence from a sufficiently fast donor–acceptor energy transfer can be superior to that from simple plasmon enhancement of the luminescence alone.

RESULTS AND DISCUSSION

To make a systematic comparison of the plasmon enhancement of luminescence in Mn-doped and undoped QDs, under the same environment and with the same average QD–MNP distance, a multilayered structure schematically shown in Figure 1a was fabricated using layer-by-layer assembly. Layers of Ag MNPs and QDs separated by a series of polyelectrolyte spacer layers were deposited on a Si substrate employing a previously reported procedure.[1,23] The details of the fabrication and characterization of the structures used are described in the Methods section. Briefly, patterned stripes of a single layer of Ag MNP (~10 nm in diameter) was initially deposited on a Si substrate using a microcontact printed pattern of (3-aminopropyl)-triethoxysilane (APTES) as the linker between the Si substrate and Ag MNPs.[24] As demonstrated in our recent work, this structure creates regions with and without plasmon enhancement on the same substrate with minimal variation of the dielectric environment, enabling a robust measurement of the luminescence enhancement.[23] Figure 1b shows the AFM image of the Ag MNP-patterned Si substrate. The distance between the QD and MNP layers was varied by changing the spacer layer thickness (*t*). A 1:1 mixture of Mn-doped and undoped CdS/ZnS QDs of the same diameter and surface passivation was used to form the top QD layer.

Figure 2 compares the absorption and luminescence spectra of Mn-doped and undoped CdS/ZnS QDs and the extinction spectrum of the Ag MNPs. Both Mn-doped and undoped QDs exhibit nearly identical absorption spectra, consistent with having the same particle size observed in TEM (Supporting Information). The absorption coefficients of the doped and undoped QDs near the band-edge exciton absorption are also nearly identical based on elemental analysis.[21] This ensures that both the doped and undoped QDs behave identically in the photoexcitation process. The plasmon resonance of the Ag MNPs near 400 nm overlaps well with the band-edge exciton absorption of the QDs centered at 420 nm. Exciton luminescence from the undoped QDs is centered at 440 nm close to the exciton band-edge absorption peak, while Mn luminescence from Mn-doped QDs is significantly more red-shifted, occurring at ~600 nm. Due to the very efficient exciton–Mn energy transfer occurring on a few picoseconds time scale, Mn-doped QDs used in this study exhibit only Mn luminescence without

exciton luminescence. The spectral overlap integral J, defined as $\int F_d(\lambda)\,\varepsilon_a(\lambda)\lambda^4\,d\lambda$, where $F_d(\lambda)$ and $\varepsilon_a(\lambda)$ are the normalized luminescence spectrum of donor and the molar extinction spectrum of Ag MNP, respectively, was 2 orders of magnitude smaller for Mn luminescence compared to the exciton luminescence.

Figure 3a and b show the representative false-color images of the luminescence intensity from the fabricated multilayered structures under 405 nm excitation at two chosen spacer layer thicknesses (t), t = 3 (a) and 9 nm (b). The luminescence was imaged with a CCD camera and bandpass filters centered at 450 and 600 nm for exciton and Mn luminescence, respectively. The line profiles of the intensity ratio (I/I_0) are also shown below each luminescence intensity image, where I and I_0 are the intensities from the regions with and without Ag MNPs, respectively. Figure 3c compares I/I_0 with varying spacer layer thicknesses for both exciton (blue) and Mn luminescence (red). The maximum net enhancement occurs at a spacer layer thickness of t = 9 nm for both exciton and Mn luminescence.

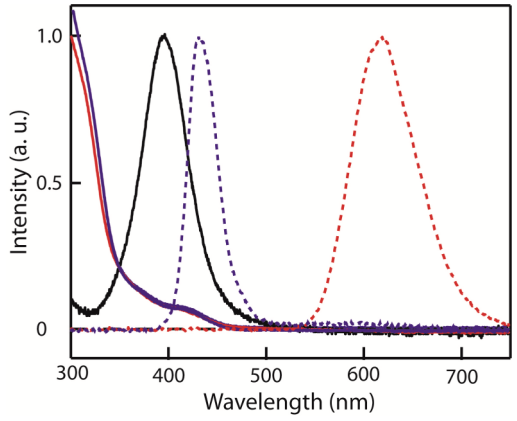

Figure 2. Comparison of the absorption (solid lines) and luminescence (dashed lines) spectra of the Mn-doped (red) and the undoped (blue) CdS/ZnS QDs. Extinction spectrum of the Ag MNPs is shown as a black solid line. The QD luminescence and Ag MNP extinction spectra are normalized.

At this thickness, the Mn luminescence exhibits a stronger net enhancement than the exciton. With increasing thickness I/I_0 gradually decreases, while maintaining a net enhancement of the luminescence. At shorter spacer layer thicknesses (*e.g.*, t < 5 nm), where the MNP-induced quenching of the luminescence outweighs the plasmon-enhanced excitation, the luminescence exhibits net quenching; that is, I/I_0 is <1. Notably at the shortest spacer layer of t < 2 nm, the Mn luminescence exhibits a stronger net quenching than exciton luminescence in contrast to the stronger net enhancement observed at t = 9 nm. The comparison of the effect of the Ag MNP/polyelectrolyte layer on the reflection and scattering efficiency of the Si substrate at 450 and 600 nm indicates that the presence of the multilayer structure does not introduce any wavelength dependence of the overall luminescence photon collection efficiency (see Supporting Information). Therefore, the difference in I/I_0 in Figure 3c reflects the actual differences in net plasmon enhancement of the two different emitters.

The important feature in Figure 3c is the stronger net enhancement (at t = 9 nm) and stronger net quenching (at t < 2 nm) of Mn luminescence compared to exciton luminescence, despite the same level of excitation enhancement in both doped and undoped QDs. The observed difference in I/I_0 between doped and undoped QDs can be attributed to the following factors: (i) differences in the MNP-induced quenching of exciton and Mn and (ii) competition between exciton−Mn energy transfer and other exciton relaxation channels. To obtain a better understanding of the different behaviors of I/I_0 observed for the doped and undoped QDs, we used a kinetic model shown in Figure 4a that includes all the major competing processes in the doped and undoped QDs adjacent to Ag MNP. In this model, $k_{r,i}$, $k_{nr,i}$, $k_{Q,i}$ (i = ex, Mn) represent the rate constants for the radiative relaxation, nonradiative relaxation in the absence of Ag MNP and quenching by Ag MNP, respectively, for both exciton

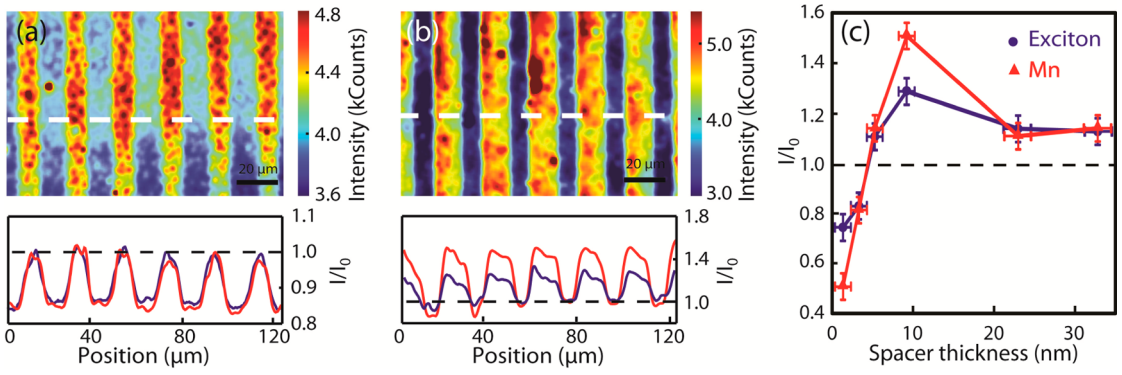

Figure 3. False-color images of Mn luminescence from the multilayered structure shown in Figure 1 with spacer layer thickness of 3 nm (a) and 9 nm (b). The bottom panels show the line profile of the intensity ratio (I/I_0) for Mn (red) and exciton (blue) luminescence at the region indicated with white dashed lines vertically averaged over 20 μm. (c) I/I_0 for exciton and Mn luminescence at different spacer layer thicknesses (t).

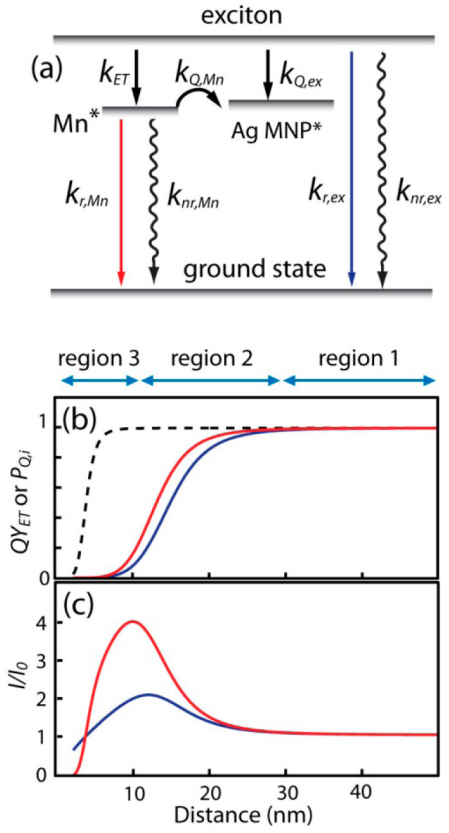

Figure 4. (a) Kinetic scheme of the photophysical processes in Mn-doped QD adjacent to Ag MNP. (b) *d*-Dependence of QY_{ET} (dashed), $P_{Q,Mn}$ (red), and $P_{Q,ex}$ (blue) in eqs 1 and 2. See the text for the parameters used for this plot. (c) *d*-Dependence of I/I_0 for Mn (red) and exciton (blue) luminescence calculated from eqs 1 and 2 using the same set of parameters used in (b).

(i = ex) and the excited state of Mn (i = Mn). Here, k_{ET} represents the rate constant for exciton−Mn intraparticle energy transfer in Mn-doped QDs. In this model, we excluded the plasmon enhancement of the radiative decay rate of the exciton in the consideration of the factors contributing to the enhancement of luminescence intensity. In principle, the MNP plasmon can enhance both the excitation rate and the radiative decay rate to varying degrees depending on the details of the geometry of the plasmonic structure and the spectral overlap between the interacting transitions and excitation wavelength.[25,26] Under our experimental conditions, where the spectral overlap is maximized among excitation wavelength, the plasmon of the isolated colloidal Ag MNP, and exciton absorption of the QD, the enhancement of radiative decay of the exciton is considered to be significantly less important than the excitation enhancement. This assumption is supported by the earlier studies that examined the enhancement of the local electric field and radiative decay rate of an emitter by the colloidal Ag MNPs, where the enhancement of the radiative decay rate was significantly weaker than enhancement of the local electric field at the relevant QD−MNP distances of this study.[27] While the model can be more refined with the inclusion of the enhancement of radiative decay rate, we used the simplified model excluding it since the essential features of the data shown in Figure 3c can be captured with less complexity of the model. In addition, in our study with randomly oriented dipoles of an ensemble of QDs, the magnitude of plasmon enhancement is averaged over many different dipole orientations with respect to the electric field. Therefore, the dipole considers only the average plasmon enhancement without explicit consideration of the dependence of the dipole orientation.

In the undoped QDs, the relative enhancement of exciton luminescence by the Ag MNP located at distance d from QD, $I_{ex}(d)/I_0$, is determined by the excitation enhancement factor ($P_{E,ex}$) and quenching factor ($P_{Q,ex}$) for the exciton luminescence as shown in eq 1. $P_{E,ex}$ represents the excitation enhancement by the plasmon-enhanced local electric field. The quenching factor for the exciton, $P_{Q,ex}$, can be expressed as the ratio of the rate constants of all the competing processes,[28] where only $k_{Q,ex}$ depends on d. $P_{Q,ex}$ is often expressed as $1/(1 + (R_{Q,ex}/d)^n)$, where $R_{Q,ex}$ is the distance at which $k_{Q,ex}(d) = k_{r,ex} + k_{nr,ex}$ and n varies between 3 and 6 depending on the geometric arrangements of interacting dipoles.[29−32]

$$\begin{aligned} I_{ex}(d)/I_0 &= P_{E,ex}(d)\, P_{Q,ex}(d) \\ &= P_{E,ex}(d)\left(\frac{k_{r,ex} + k_{nr,ex}}{k_{r,ex} + k_{nr,ex} + k_{Q,ex}(d)}\right) \\ &= P_{E,ex}(d)\left(\frac{1}{1 + (R_{Q,ex}/d)^n}\right) \end{aligned} \quad (1)$$

$$\begin{aligned} I_{Mn}(d)/I_0 &= P_{E,ex}(d)\, QY_{ET}(d)\, P_{Q,Mn}(d) \\ &= P_{E,ex}(d)\left(\frac{k_{ET}}{k_{r,ex} + k_{nr,ex} + k_{Q,ex}(d) + k_{ET}}\right) \\ &\quad \times \left(\frac{k_{r,Mn} + k_{nr,Mn}}{k_{r,Mn} + k_{nr,Mn} + k_{Q,Mn}(d)}\right) \\ &\approx P_{E,ex}(d)\left(\frac{1}{1 + (R_{ET}/d)^n}\right)\left(\frac{1}{1 + (R_{Q,Mn}/d)^{n'}}\right) \end{aligned} \quad (2)$$

In Mn-doped QDs, $I_{Mn}(d)/I_0$ is determined by the excitation enhancement factor for the exciton ($P_{E,ex}$), exciton−Mn energy transfer quantum yield (QY_{ET}) in the presence of a Ag MNP and the quenching factor for Mn luminescence ($P_{Q,Mn}$) as described in eq 2. Both the doped and undoped QDs have the same $P_{E,ex}$, since their absorption spectra near the band-edge are identical. $P_{Q,Mn}$ is expressed as the ratio of the rate constants of the relevant competing processes or in terms of $R_{Q,Mn}$ defined similar to $R_{Q,ex}$. Here, $R_{Q,Mn}$ represents the average behavior of many Mn^{2+} ions doped in the QD. The energy transfer quantum yield (QY_{ET}) can also

be expressed as the ratio of the rate constants. Since $k_{ET} \gg k_{r,ex} + k_{nr,ex}$ for Mn-doped QDs used in this study,[20,21] QY_{ET} can be approximated as $1/(1 + (R_{ET}/d)^n)$, where R_{ET} is the distance at which $k_{Q,ex}(d) = k_{ET}$. For the Mn-doped QDs used in this study, k_{ET} was $\sim 2.5 \times 10^{11}$ s^{-1}, which is 1−2 orders of magnitude larger than $k_{r,ex} + k_{nr,ex}$ according to our recent study on the dynamics of energy transfer in Mn-doped QDs.[20,21]

The observed stronger net enhancement or net quenching of Mn luminescence compared to the exciton luminescence shown in Figure 3c can be explained with this model when the following two conditions are met: (i) exciton−Mn energy transfer is much faster than exciton relaxation ($k_{ET} \gg k_{r,ex}+k_{nr,ex}$) and (ii) the Mn excited state experiences less MNP-induced quenching than the exciton, i.e., $P_{Q,Mn}(d) > P_{Q,ex}(d)$. The first condition is readily met in the doped QDs used in this study as mentioned above. The second condition is expected to be satisfied because of the weaker donor−acceptor spectral overlap of the Mn−MNP pair than in the exciton−MNP pair if the dominant quenching mechanism involves energy transfer to the localized surface plasmon of Ag MNP. When these two conditions are met, it follows that $R_{ET} < R_{Q,Mn} < R_{Q,ex}$ if the quenching mechanism is the same for both Mn and exciton luminescence, *i.e.*, $n = n'$. The corresponding distance dependence of QY_{ET}, $P_{Q,Mn}$, $P_{Q,ex}$, and the resulting I/I_0 are shown in Figure 4b and c, respectively. The curves in these plots were calculated with the following set of parameters for the qualitative comparison with the experimental data rather than showing the fit to the experimentally measured I/I_0: $R_{ET} = 3.7$ nm, $R_{Q,Mn} = 13$ nm, $R_{Q,ex} = 14.8$ nm, $n = n' = 6$. The details of the choice of the parameters in this analysis and the limitation of the model are described in the Supporting Information.

Below we examine the different distance dependence of I/I_0 for exciton and Mn luminescence in more detail. At large QD−MNP distances (region 1), where the quenching is negligible compared to the other competing processes, both $P_{Q,ex}$ and $P_{Q,Mn}$ are close to 1. QY_{ET} is also close to 1 in this regime since $k_{ET} \gg k_{Q,ex}$. Therefore, both exciton and Mn luminescence exhibit similar I/I_0, which is slightly larger than 1. At shorter QD−MNP distances, where the quenching is not negligible, I/I_0 of the Mn and exciton luminescence will behave differently depending on the relative magnitudes of $P_{Q,ex}$ and $QY_{ET}P_{Q,Mn}$. At intermediate QD−MNP distances (region 2), where QY_{ET} is still close to 1, the Mn luminescence can take maximum advantage of the plasmon-enhanced excitation and the comparatively weaker luminescence quenching than that of the exciton. The experimentally observed behavior in Figure 3c near t = 9 nm belongs to this regime. As the QD−MNP distance continues to decrease (region 3), the rapid drop in QY_{ET} offsets the advantage of the weaker quenching of Mn, eventually leading to stronger net luminescence quenching of the Mn than the exciton. Such behavior is observed in Figure 3c at $t < 2$ nm. The model described by eqs 1 and 2 successfully describes the observation qualitatively. On the other hand, this model overestimates the dependence of I/I_0 on the thickness of the spacer layer, since it does not account for the distribution of the QD−MNP interparticle distances inherent in the multilayer structures used in this study (see Supporting Information). The distribution of the QD−MNP distances partially smears out the distance dependence of I/I_0, which results in the less pronounced dependence of the experimentally measured I/I_0 on the spacer layer thickness than the model predicts. The above analysis suggests that other donor−acceptor systems exhibiting sensitized luminescence from a sufficiently fast energy transfer may also benefit from the reduced MNP-induced quenching. In the case of the Mn-doped QDs, such a benefit has more practical significance, since the Mn luminescence is often stronger and more robust than exciton luminescence even without the plasmon enhancement.[22,33]

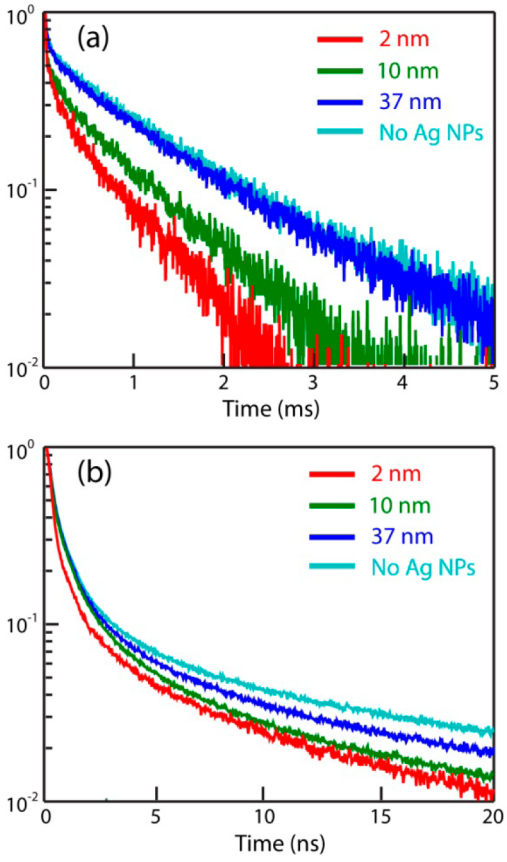

Figure 5. Time-resolved (a) Mn and (b) exciton luminescence intensity at various polymer spacer layer thicknesses.

We also attempted to gain further insights into the difference in MNP quenching of exciton and Mn luminescence by measuring the time-resolved luminescence intensities as a function of the spacer layer thickness (t). Figure 5a and b show the semilog plots of the normalized time-resolved Mn and exciton luminescence intensities respectively at varying values of t.

TABLE 1. Average Luminescence Lifetime of Exciton (τ_{ex}) and Mn (τ_{Mn}) from the Undoped and Mn-Doped QDs, Respectively, at Varying Spacer Layer Thicknesses (t)

t	τ_{ex} (ns)	τ_{Mn} (ms)
no Ag MNP[a]	17.41	1.91
37 nm	16.68	1.78
10 nm	12.88	1.22
2 nm	4.78	0.96

[a] Lifetime measured on Si substrates without underlying Ag MNP layer.

For this measurement, the entire area of the Si substrate was covered with Ag MNPs, and the rest of the multilayer structure was fabricated identically to the one shown in Figure 1a. The average lifetime decreases with the decrease of the spacer layer thickness for both exciton (τ_{ex}) and Mn (τ_{Mn}) luminescence as summarized in Table 1. Both τ_{ex} and τ_{Mn} exhibit a comparable relative decrease as the spacer layer thickness changes from t = 37 to 10 nm. On the other hand, τ_{Mn} decreases significantly less than τ_{ex} at t = 2 nm. This indicates that the quenching effect of Ag MNP on luminescence is weaker in Mn than for the exciton at this spacer layer thickness, consistent with our expectation. However, it is not straightforward to quantitatively measure the quenching kinetics as a function of QD–MNP distance from the time-resolved luminescence data obtained from the multilayer structure due to the heterogeneity of the quenching kinetics. There are two main sources of the heterogeneity influencing the MNP-induced quenching kinetics in the multilayer structure used in this study. One is the distribution of QD–MNP interparticle distances (d) for a given spacer layer thickness (t) as discussed earlier. The other is the migration of the emitting states within the QD layer, which is unequal between the exciton and Mn excited states. Excitons in undoped QDs can migrate away from the initial excitation site *via* interparticle Förster resonance energy transfer (FRET) in a relatively close-packed QD layer.[34−37] This can distort the distance dependence of the quenching kinetics especially when the Ag MNP layer is not close packed. The comparison of the time-resolved exciton luminescence in both solution and film samples indicates that interparticle FRET in the layer of QD film occurs on the ~ns time scale[34,38] (see Supporting Information). Trapping of the exciton by various different trap sites at different energy levels adds an additional complexity to the interpretation of time-dependent luminescence data. The trapping of the exciton and thermal detrapping result in multiexponential decay of the luminescence and is often responsible for a slow decay component in time-resolved luminescence data since the detrapping of the exciton acts as a slowly leaking source of exciton luminescence. Such complexity also makes it difficult to define a single average lifetime of exciton that can readily be used in the evaluation of the quantum yield that usually assumes the competition among the first-order (single-exponential) processes. On the other hand, the Mn excited state is highly localized on the Mn^{2+} ion and stays within the initially excited QD due to very rapid exciton–Mn energy transfer.[39] The fact that the solution and dense film samples of Mn-doped QDs exhibit the identical luminescence decay indicates the absence of migration of the Mn excited state *via* FRET. Studies of isolated QD–MNP pairs with known interparticle distances are needed to obtain more accurate kinetic information.

One interesting observation from the time-resolved luminescence measurements is that MNP-induced quenching of the Mn luminescence is still quite substantial, while it is weaker than in the exciton luminescence. Since the spectral overlap integral J of Mn–Ag MNP is 2 orders of magnitude smaller than that of the exciton–Ag MNP, $R_{Q,Mn}$ should be approximately half of $R_{Q,ex}$ assuming the quenching of luminescence *via* FRET, where the Förster distance is proportional to $J^{1/6}$.[40] In this case, eq 1 and eq 2 predict a much stronger suppression of the Mn luminescence quenching than was observed experimentally. This suggests that an additional quenching mechanism that is less sensitive to the donor–acceptor spectral overlap integral, such as quenching *via* electron–hole excitation near the Fermi level, may be partially involved in quenching of Mn luminescence.[32]

CONCLUSION

In this study, we showed that sensitized Mn luminescence arising from the fast exciton–dopant energy transfer occurring on a few picoseconds time scale exhibits a stronger plasmon enhancement of luminescence than the exciton due to a suppression of MNP-induced quenching of the luminescence. The rapid energy transfer that separates the absorber (exciton) and emitter (Mn) in time can partially separate the plasmon enhancement of the excitation from the MNP-induced quenching processes, both of which results from the presence of the plasmonic MNPs. When combined with the reduced spectral overlap between the sensitized Mn luminescence and MNP plasmon, as compared to the exciton luminescence, the Mn luminescence in Mn-doped QDs exhibited a stronger net plasmon enhancement than the exciton at the optimum separation between the MNP and QD layers.

METHODS

Synthesis of the Mn-Doped and Undoped CdS/ZnS Core/Shell Quantum Dots. Mn-doped and undoped CdS/ZnS core/shell QDs were synthesized following previously reported procedures.[21,41,42] Briefly, the CdS core was synthesized by injecting 2.0 mL of octadecene (ODE) solution with sulfur (0.25 M) to a mixture of ODE (12.0 mL), CdO (125 mg), and oleic acid (2.02 g) at 250 °C and growing at 240 °C. The rinsed CdS core was further coated

with a ZnS shell *via* the SILAR (successive ionic layer adsorption and reaction) procedure using ODE solutions of sulfur (0.25 M) and zinc stearate (0.25 M) as the precursors. Doping with Mn^{2+} ions was achieved by adding a Mn precursor (manganese diethyldithiocarbamate in oleylamine) at the chosen step during the SILAR process. In this study, Mn^{2+} ions were doped at the interface of the CdS core (1.8 nm in radius) and ZnS shell (1.8 nm in thickness). Since the cation and anion layers are added sequentially, the step at which the Mn precursor is introduced determines the radial location of the dopant. Details of the doping procedure can be found elsewhere.[21] In order to make the water-soluble QDs required for the deposition of the QD layer from the aqueous solution, ligand exchange was performed to replace the original surfactant with mercaptoundecanoic acid (MUA). The ligand exchange was performed by adding the QDs into a mixture of methanol, acetone, and MUA at pH 10 adjusted with tetramethylammonium hydroxide. The resulting MUA-passivated QDs were precipitated and rinsed with a 1:1 mixture of ethyl acetate and petroleum ether before finally redispersed in Millipore water.

Fabrication and Characterization of the Multilayered Structure on the Ag MNP-Patterned Substrate. Clean Si(111) substrates were prepared by immersing the wafer in piranha solution at 100 °C for 1 h and rinsing with Millipore water. To make the stripe-patterned layer of APTES used as the linker between the substrate and Ag MNPs, the microcontact printing method was used.[24] The polydimethylsiloxane (PDMS) stamps used for this purpose were made using a Si template having 12 μm wide stripe patterns with a pitch of 9 μm. The inking of the PDMS stamp with APTES was done by dropping a 1% aqueous solution of APTES on top of the stamp. After removing the excess APTES solution with dry nitrogen from the PDMS stamp, a patterned APTES layer was transferred to the Si substrate by making a direct contact between the stamp and the substrate. The APTES-patterned Si substrate was dried for 1 h and subsequently immersed in the aqueous solution of Ag MNPs (Sigma-Aldrich, 10 nm in diameter) for 45 min to allow the selective adsorption of Ag MNPs to the APTES-coated region. After rinsing the substrate with Millipore water, the resulting structure on the Si substrates was patterned stripes of Ag MNPs. A representative topographic image of the patterned Ag MNP layer on the Si substrate obtained with an atomic force microscope (AFM, Agilent Technologies 5500) is shown in Figure 1b. The polyelectrolyte spacer layer that separates the Ag MNP layer and QD layer was formed on top of the Ag MNP layer using a layer-by-layer deposition method.[1,23] Oppositely charged layers of poly(diallyldimethylammonium chloride) and poly(sodium 4-styrenesulfonate) were alternately deposited from 0.5 M NaCl solutions of the polyelectrolyte. The thickness of the spacer layer was changed by varying the total number of layers deposited. The thickness of the spacer layer was measured from the topographic AFM images of the covered *versus* uncovered regions of the substrate obtained with a WITec Alpha 300 AFM (see Supporting Information). The roughness of the polyelectrolyte layer surface in the AFM image is *ca.* $\pm$1 nm, while the actual surface roughness could be larger due to the finite lateral dimension of the AFM tip. The QD layer was deposited on top of the outermost spacer layer by dipping the substrate in the aqueous solution of a 1:1 mixture of Mn-doped and undoped QDs for ~1 min and rinsing the substrate thoroughly with Millipore water. All AFM images were acquired under ambient conditions in tapping mode using commercially available aluminum-coated silicon AFM tips from Nanoscience Instruments (Phoenix, AZ, USA) with nominal tip radii of less than 10 nm and nominal spring constants of 48 N/m.

Imaging of Plasmon-Enhanced Luminescence Intensity on the Patterned Structure. The luminescence from the QD layer formed on the Si substrate was imaged with a home-built microscope constructed with a 50× objective (Nikon, CFI L Plan EPI SLWD) and a tube lens (Nikon, f = 200 mm). A liquid nitrogen-cooled CCD (Princeton Instruments, PI-LCX) was used as the imaging device, and a 405 nm CW diode laser (Crystalaser) was used as the excitation source. The laser beam directly illuminated the entire imaging area (0.5 × 0.5 mm^2) of the Si substrate. The detailed construction and arrangement of the optical elements in this setup are described in the Supporting Information. A long-pass filter (410 nm) was used to block the excitation light reaching the CCD. Bandpass filters centered at 450 nm (fwhm = 60 nm) and 600 nm (fwhm = 10 nm) were used to record the images of exciton and Mn luminescence, respectively.

Time-Resolved Luminescence Intensity Measurements. The time-resolved luminescence was measured using two different methods. For the Mn luminescence, a pulsed nitrogen laser (Stanford Research Systems, NL100, 3.5 ns pulse width) centered at 337 nm and photomultiplier tube (Hamamatsu, 982R) were used in conjunction with a digital oscilloscope (LeCroy, WaveAce). A 500 nm long-pass filter was used to prevent the excitation light from reaching the detector. For the exciton luminescence, a time-correlated single photon counting (TCSPC) technique was used to measure the time-resolved luminescence. A pulsed diode laser (Picoquant, 80 ps pulse width) centered at 405 nm operating at 10 MHz was used as the excitation source. The exciton luminescence filtered with a 450 nm bandpass filter (fwhm = 50 nm) was detected with a TCSPC-enabled PMT, with channel binning of 32 ps over the full time window (100 ns) of the measurement. The time-resolved exciton luminescence was obtained at several different areas on the substrate on a confocal microscope (Olympus, FV-1000) using a fluorescence lifetime imaging technique. The average lifetimes (τ_{av}) reported in Table 1 are $\tau_{av} = \Sigma(a_i\tau_i^2)/\Sigma(a_i\tau_i)$, where a_i and τ_i are the amplitude and time constant obtained from the multiexponential fit of the data.

Conflict of Interest: The authors declare no competing financial interest.

Acknowledgment. This work was supported by the Robert A. Welch Foundation (A-1639) to D.H.S. and the National Science Foundation (CHE-0848786) to J.D.B. Portions of this work were facilitated by use of instrumentation in the Laboratory for Synthetic-Biologic Interactions directed by Prof. Karen L. Wooley, which was supported by the Robert A. Welch Foundation (A-0001).

Supporting Information Available: Details of materials for the synthesis, the collection efficiency test for the multilayered construct, determination of the parameters in the model for *d*-dependence of the plasmon-enhanced luminescence, the characterization of the multilayered construct, comparison of the time-resolved exciton and Mn luminescence between dilute solution and thin film samples, and the optical setup for the luminescence intensity measurement are available free of charge *via* the Internet at http://pubs.acs.org.

REFERENCES AND NOTES

1. Kulakovich, O.; Strekal, N.; Yaroshevich, A.; Maskevich, S.; Gaponenko, S.; Nabiev, I.; Woggon, U.; Artemyev, M. Enhanced Luminescence of CdSe Quantum Dots on Gold Colloids. *Nano Lett.* **2002**, *2*, 1449–1452.
2. Govorov, A. O.; Bryant, G. W.; Zhang, W.; Skeini, T.; Lee, J.; Kotov, N. A.; Slocik, J. M.; Naik, R. R. Exciton–Plasmon Interaction and Hybrid Excitons in Semiconductor–Metal Nanoparticle Assemblies. *Nano Lett.* **2006**, *6*, 984–994.
3. Ni, W.; Ambjörnsson, T.; Apell, S. P.; Chen, H.; Wang, J. Observing Plasmonic–Molecular Resonance Coupling on Single Gold Nanorods. *Nano Lett.* **2009**, *10*, 77–84.
4. Achermann, M. Exciton–Plasmon Interactions in Metal–Semiconductor Nanostructures. *J. Phys. Chem. Lett.* **2010**, *1*, 2837–2843.
5. Ming, T.; Chen, H.; Jiang, R.; Li, Q.; Wang, J. Plasmon-Controlled Fluorescence: Beyond the Intensity Enhancement. *J. Phys. Chem. Lett.* **2011**, *3*, 191–202.
6. Saboktakin, M.; Ye, X.; Oh, S. J.; Hong, S.-H.; Fafarman, A. T.; Chettiar, U. K.; Engheta, N.; Murray, C. B.; Kagan, C. R. Metal-Enhanced Upconversion Luminescence Tunable through Metal Nanoparticle–Nanophosphor Separation. *ACS Nano* **2012**, *6*, 8758–8766.
7. Yates, C. J.; Samuel, I. D. W.; Burn, P. L.; Wedge, S.; Barnes, W. L. Surface Plasmon-Polariton Mediated Emission from Phosphorescent Dendrimer Light-Emitting Diodes. *Appl. Phys. Lett.* **2006**, *88*, 161105–3.

8. Choulis, S. A.; Mathai, M. K.; Choong, V.-E. Influence of Metallic Nanoparticles on the Performance of Organic Electrophosphorescence Devices. *Appl. Phys. Lett.* **2006**, *88*, 213503–3.
9. Kwon, M.-K.; Kim, J.-Y.; Kim, B.-H.; Park, I.-K.; Cho, C.-Y.; Byeon, C. C.; Park, S.-J. Surface-Plasmon-Enhanced Light-Emitting Diodes. *Adv. Mater.* **2008**, *20*, 1253–1257.
10. Kelly, K. L.; Coronado, E.; Zhao, L. L.; Schatz, G. C. The Optical Properties of Metal Nanoparticles: The Influence of Size, Shape, and Dielectric Environment. *J. Phys. Chem. B* **2002**, *107*, 668–677.
11. Halas, N. J.; Lal, S.; Chang, W.-S.; Link, S.; Nordlander, P. Plasmons in Strongly Coupled Metallic Nanostructures. *Chem. Rev.* **2011**, *111*, 3913–3961.
12. Daniel, M.-C.; Astruc, D. Gold Nanoparticles: Assembly, Supramolecular Chemistry, Quantum-Size-Related Properties, and Applications toward Biology, Catalysis, and Nanotechnology. *Chem. Rev.* **2003**, *104*, 293–346.
13. Jones, M. R.; Osberg, K. D.; Macfarlane, R. J.; Langille, M. R.; Mirkin, C. A. Templated Techniques for the Synthesis and Assembly of Plasmonic Nanostructures. *Chem. Rev.* **2011**, *111*, 3736–3827.
14. Rycenga, M.; Cobley, C. M.; Zeng, J.; Li, W.; Moran, C. H.; Zhang, Q.; Qin, D.; Xia, Y. Controlling the Synthesis and Assembly of Silver Nanostructures for Plasmonic Applications. *Chem. Rev.* **2011**, *111*, 3669–3712.
15. Dulkeith, E.; Morteani, A. C.; Niedereichholz, T.; Klar, T. A.; Feldmann, J.; Levi, S. A.; van Veggel, F. C. J. M.; Reinhoudt, D. N.; Möller, M.; Gittins, D. I. Fluorescence Quenching of Dye Molecules near Gold Nanoparticles: Radiative and Nonradiative Effects. *Phys. Rev. Lett.* **2002**, *89*, 203002.
16. Soller, T.; Ringler, M.; Wunderlich, M.; Klar, T. A.; Feldmann, J.; Josel, H. P.; Markert, Y.; Nichtl, A.; Kürzinger, K. Radiative and Nonradiative Rates of Phosphors Attached to Gold Nanoparticles. *Nano Lett.* **2007**, *7*, 1941–1946.
17. Eichelbaum, M.; Rademann, K. Plasmonic Enhancement or Energy Transfer? On the Luminescence of Gold-, Silver-, and Lanthanide-Doped Silicate Glasses and Its Potential for Light-Emitting Devices. *Adv. Funct. Mater.* **2009**, *19*, 2045–2052.
18. Viste, P.; Plain, J.; Jaffiol, R.; Vial, A.; Adam, P. M.; Royer, P. Enhancement and Quenching Regimes in Metal–Semiconductor Hybrid Optical Nanosources. *ACS Nano* **2010**, *4*, 759–764.
19. Pillonnet, A.; Berthelot, A.; Pereira, A.; Benamara, O.; Derom, S.; Francs, G. C. d.; Jurdyc, A.-M. Coupling Distance between Eu^{3+} Emitters and Ag Nanoparticles. *Appl. Phys. Lett.* **2012**, *100*, 153115.
20. Chen, H.-Y.; Chen, T.-Y.; Son, D. H. Measurement of Energy Transfer Time in Colloidal Mn-Doped Semiconductor Nanocrystals. *J. Phys. Chem. C* **2010**, *114*, 4418–4423.
21. Chen, H.-Y.; Maiti, S.; Son, D. H. Doping Location-Dependent Energy Transfer Dynamics in Mn-Doped CdS/ZnS Nanocrystals. *ACS Nano* **2011**, *6*, 583–591.
22. Beaulac, R.; Archer, P. I.; Gamelin, D. R. Luminescence in Colloidal Mn^{2+}-Doped Semiconductor Nanocrystals. *J. Solid State Chem.* **2008**, *181*, 1582–1589.
23. Chan, Y.-H.; Chen, J.; Wark, S. E.; Skiles, S. L.; Son, D. H.; Batteas, J. D. Using Patterned Arrays of Metal Nanoparticles to Probe Plasmon Enhanced Luminescence of CdSe Quantum Dots. *ACS Nano* **2009**, *3*, 1735–1744.
24. Li, H.; Zhang, J.; Zhou, X.; Lu, G.; Yin, Z.; Li, G.; Wu, T.; Boey, F.; Venkatraman, S. S.; Zhang, H. Aminosilane Micropatterns on Hydroxyl-Terminated Substrates: Fabrication and Applications. *Langmuir* **2009**, *26*, 5603–5609.
25. Chen, Y.; Munechika, K.; Plante, I. J.-L.; Munro, A. M.; Skrabalak, S. E.; Xia, Y.; Ginger, D. S. Excitation Enhancement of CdSe Quantum Dots by Single Metal Nanoparticles. *Appl. Phys. Lett.* **2008**, *93*, 053106–3.
26. Munechika, K.; Chen, Y.; Tillack, A. F.; Kulkarni, A. P.; Plante, I. J.-L.; Munro, A. M.; Ginger, D. S. Spectral Control of Plasmonic Emission Enhancement from Quantum Dots near Single Silver Nanoprisms. *Nano Lett.* **2010**, *10*, 2598–2603.
27. Carminati, R.; Greffet, J. J.; Henkel, C.; Vigoureux, J. M. Radiative and Non-Radiative Decay of a Single Molecule Close to a Metallic Nanoparticle. *Opt. Commun.* **2006**, *261*, 368–375.
28. Valeur, B. Effects of Intermolecular Photophysical Processes on Fluorescence Emission. In *Molecular Fluorescence*; Wiley-VCH Verlag GmbH, 2001; pp 72–124.
29. Yun, C. S.; Javier, A.; Jennings, T.; Fisher, M.; Hira, S.; Peterson, S.; Hopkins, B.; Reich, N. O.; Strouse, G. F. Nanometal Surface Energy Transfer in Optical Rulers, Breaking the FRET Barrier. *J. Am. Chem. Soc.* **2005**, *127*, 3115–3119.
30. Pons, T.; Medintz, I. L.; Sapsford, K. E.; Higashiya, S.; Grimes, A. F.; English, D. S.; Mattoussi, H. On the Quenching of Semiconductor Quantum Dot Photoluminescence by Proximal Gold Nanoparticles. *Nano Lett.* **2007**, *7*, 3157–3164.
31. Govorov, A. O.; Lee, J.; Kotov, N. A. Theory of Plasmon-Enhanced Förster Energy Transfer in Optically Excited Semiconductor and Metal Nanoparticles. *Phys. Rev. B* **2007**, *76*, 125308.
32. Persson, B. N. J.; Lang, N. D. Electron-Hole-Pair Quenching of Excited States near a Metal. *Phys. Rev. B* **1982**, *26*, 5409–5415.
33. Pradhan, N.; Battaglia, D. M.; Liu, Y.; Peng, X. Efficient, Stable, Small, and Water-Soluble Doped ZnSe Nanocrystal Emitters as Non-Cadmium Biomedical Labels. *Nano Lett.* **2006**, *7*, 312–317.
34. Kagan, C. R.; Murray, C. B.; Nirmal, M.; Bawendi, M. G. Electronic Energy Transfer in CdSe Quantum Dot Solids. *Phys. Rev. Lett.* **1996**, *76*, 1517–1520.
35. Kagan, C. R.; Murray, C. B.; Bawendi, M. G. Long-Range Resonance Transfer of Electronic Excitations in Close-Packed CdSe Quantum-Dot Solids. *Phys. Rev. B* **1996**, *54*, 8633–8643.
36. Komarala, V. K.; Bradley, A. L.; Rakovich, Y. P.; Byrne, S. J.; Gun'ko, Y. K.; Rogach, A. L. Surface Plasmon Enhanced Förster Resonance Energy Transfer between the CdTe Quantum Dots. *Appl. Phys. Lett.* **2008**, *93*, 123102–3.
37. Rogach, A. L.; Klar, T. A.; Lupton, J. M.; Meijerink, A.; Feldmann, J. Energy Transfer with Semiconductor Nanocrystals. *J. Mater. Chem.* **2009**, *19*, 1208–1221.
38. Crooker, S. A.; Hollingsworth, J. A.; Tretiak, S.; Klimov, V. I. Spectrally Resolved Dynamics of Energy Transfer in Quantum-Dot Assemblies: Towards Engineered Energy Flows in Artificial Materials. *Phys. Rev. Lett.* **2002**, *89*, 186802.
39. White, M. A.; Weaver, A. L.; Beaulac, R.; Gamelin, D. R. Electrochemically Controlled Auger Quenching of Mn^{2+} Photoluminescence in Doped Semiconductor Nanocrystals. *ACS Nano* **2011**, *5*, 4158–4168.
40. Lakowicz, J. R. *Principles of Fluorescence Spectroscopy*; Springer: Berlin, 2009.
41. Yang, Y.; Chen, O.; Angerhofer, A.; Cao, Y. C. Radial-Position-Controlled Doping in CdS/ZnS Core/Shell Nanocrystals. *J. Am. Chem. Soc.* **2006**, *128*, 12428–12429.
42. Yu, W. W.; Peng, X. Formation of High-Quality CdS and Other II–VI Semiconductor Nanocrystals in Noncoordinating Solvents: Tunable Reactivity of Monomers. *Angew. Chem., Int. Ed.* **2002**, *41*, 2368–2371.